Effects of variable properties on MHD heat and mass transfer flow near a stagnation point towards a stretching sheet in a porous medium with thermal radiation

A. M. Salem[a)†] and Rania Fathy[b)]

[a)] *Department of Basic Science, Faculty of Computer & Informatics, Suez Canal University, Egypt*
[b)] *Department of Mathematics, Faculty of Science, Zagazig University, Egypt*

(Received 13 August 2011; revised manuscript received 14 November 2011)

The effect of variable viscosity and thermal conductivity on steady magnetohydrodynamic (MHD) heat and mass transfer flow of viscous and incompressible fluid near a stagnation point towards a permeable stretching sheet embedded in a porous medium are presented, taking into account thermal radiation and internal heat genberation/absorbtion. The stretching velocity and the ambient fluid velocity are assumed to vary linearly with the distance from the stagnation point. The Rosseland approximation is used to describe the radiative heat flux in the energy equation. The governing fundamental equations are first transformed into a system of ordinary differential equations using a scaling group of transformations and are solved numerically by using the fourth-order Rung–Kutta method with the shooting technique. A comparison with previously published work has been carried out and the results are found to be in good agreement. The results are analyzed for the effect of different physical parameters, such as the variable viscosity and thermal conductivity, the ratio of free stream velocity to stretching velocity, the magnetic field, the porosity, the radiation and suction/injection on the flow, and the heat and mass transfer characteristics. The results indicate that the inclusion of variable viscosity and thermal conductivity into the fluids of light and medium molecular weight is able to change the boundary-layer behavior for all values of the velocity ratio parameter λ except for $\lambda = 1$. In addition, the imposition of fluid suction increases both the rate of heat and mass transfer, whereas fluid injection shows the opposite effect.

Keywords: variable viscosity, variable thermal conductivity, stagnation point

PACS: 44.20.+b, 44.30.+v, 44.40.+a **DOI:** 10.1088/1674-1056/21/5/054701

1. Introduction

The study of hydrodynamic stagnation point flow over a stretching surface has attracted much attention due to their many practical applications such as MHD generators and cooling of infinite metallic plates in a bath. Hiemenz[1] first studied two-dimensional stagnation flow using similarity transformations to reduce the Navier–Stokes equations to non-linear ordinary differential equations and Eckert[2] considered the corresponding heat transfer problems. Ramachandran *et al.*[3] studied laminar mixed convection in two-dimensional stagnation flows around heated surfaces by considering both an arbitrary wall temperature and a varying arbitrary surface heat flux. This work was then extended by Devi *et al.*[4] to the unsteady case, and by Lok *et al.*[5] to a vertical surface immersed in a micropolar fluid. The stagnation point flows towards a surface which has been moved or stretched have been much investigated.[6−13] In many new engineering areas where processes occur at high temperatures, radiation heat transfer besides the convective heat transfer plays a very important role and cannot be neglected. Hossain and Takhar[14] studied the effect of radiation using the Rosseland diffusion approximation, which leads to non-similar solutions for the forced and free convection flow of an optically dense fluid from vertical surfaces with constant free stream velocity and surface temperature. Pop *et al.*[15] analyzed the radiative effects on the steady two-dimensional stagnation-point flow of an incompressible fluid over a stretching sheet.

The problem of flow, heat and mass transfer in a laminar boundary layer over a stretching sheet in a saturated porous medium has an important application in the metallurgy and chemical engineering fields. Layek *et al.*[16] considered the flow and heat transfer boundary layer stagnation-point flow of an incompressible viscous fluid towards a heated porous stretching sheet embedded in a porous medium subject to suction/blowing with internal heat generation

†Corresponding author. E-mail: azizsalem32@hotmail.com
© 2012 Chinese Physical Society and IOP Publishing Ltd

or absorption. Dulal[17] has reported heat and mass transfer in stagnation-point flow towards a stretching surface in the presence of buoyancy force and thermal radiation. Recently, Adrian[18] studied heat and mass transfer by natural convection at a stagnation-point in a porous medium considering Soret and Dufour effects.

All the above mentioned investigations were carried out for fluids having constant viscosity and thermal conductivity throughout the boundary-layer. However it is known that these physical properties may change significantly with temperature. For instance, the viscosity of water decreases about 240% when the temperature increases from 10 °C to 50 °C. The viscosity of air is 0.6924×10^{-5}, 1.3289, 2.286, and 3.625 at temperatures 1000, 2000, 4000, and 8000 K respectively.[19] To predict accurately the flow behaviors, it is necessary to take the variation of viscosity and thermal conductivity into account. Chamkha[20] discussed the effect of thermal and concentration buoyancy on an unsteady two-dimensional laminar MHD flow which is heat-absorbing over a moving vertical plate. Seddeek and Salama[21] studied the effects of the variable viscosity and thermal conductivity on an unsteady two-laminar MHD flow past a vertical porous moving plate considering the effect of variable suction. Salem[22] investigated variable viscosity and thermal conductivity effects on MHD flow heat transfer in viscoelastic fluid over a stretching sheet. Hassanian *et al.*[23] investigated the steady non-Darcy mixed convection flow near the stagnation point on a heated vertical surface embedded in a porous medium with thermal radiation and variable viscosity.

The Lie-group method is applied to the non-linear partial differential equations arising in fluid mechanics, which leads to similarity variables that may be used to reduce the number of independent variables in the partial differential equations. By determining the transformation group under which a given partial differential equation is invariant, we can obtain information about the invariants and symmetries of the equations. This information can be used to determine the similarity transformations that can reduce a system of partial differential equations and associated boundary conditions to a system of ordinary differential equations.[24−28] Youssef *et al.*[29] used lie symmetry techniques to obtain similarity reductions of nonlinear boundary layer equations for two-dimensional steady flow of an incompressible viscous fluid near a stagnation point on a heated surface placed in porous medium. In the present paper, we will extend the work of Youssef *et al.*[30] and study the effect of surface mass transfer on a steady boundary layer MHD flow with heat and mass transfer near the stagnation point over a stretching sheet through a porous medium in the presence of temperature-dependent viscosity and thermal conductivity, taking into account radiation effects using the Rosseland approximation to model the radiative heat transfer. The Lie-group method is applied to the equations of motion for determining symmetry reductions of the partial differential equations. The transformed dimensionless governing equations are solved numerically by using the fourth-order Rung-Kutta with the shooting technique. The effects of the physical parameters of the problem such as velocity ratio, variable viscosity, variable thermal conductivity, magnetic field, radiation, porous medium, and surface mass transfer, are investigated in this study.

2. Mathematical analysis

Consider the steady two-dimensional MHD flow with heat and mass transfer near a stagnation-point on a stretching porous surface placed in the $y = 0$ plane of a Cartesian system, the flow is in the region $y > 0$ where the space above the plane sheet is filled with the porous medium. The velocity $u_{\rm w}(x)$ and the temperature $T_{\rm w}(x)$ of the stretching sheet are proportional to the distance x from the stagnation-point. We consider a gray, absorbing-emitting radiation fluid but a nonscattering medium, and the Rosseland approximation is used to describe the radiative heat flux in the energy equation. The fluid properties are assumed to isotropic and constant, except for the fluid viscosity and thermal conductivity. The governing equations of the mass, momentum, energy and concentration for steady flow can be written as

$$\frac{\partial u}{\partial x} + \frac{\partial v}{\partial y} = 0, \tag{1}$$

$$u\frac{\partial u}{\partial x} + v\frac{\partial u}{\partial y} = U\frac{\partial U}{\partial x} + \frac{1}{\rho_\infty}\frac{\partial}{\partial y}\Big(\mu(T)\frac{\partial u}{\partial y}\Big) + \frac{\mu(T)}{\rho_\infty K}(U-u) - \frac{\sigma B_0^2}{\rho_\infty}(U-u), \tag{2}$$

$$u\frac{\partial T}{\partial x} + v\frac{\partial T}{\partial y} = \frac{1}{\rho_\infty c_p}\frac{\partial}{\partial y}\Big(k(T)\frac{\partial T}{\partial y}\Big) + \frac{Q_0}{\rho_\infty c_p}(T-T_\infty) - \frac{1}{\rho_\infty c_p}\frac{\partial q_{\rm r}}{\partial y}, \tag{3}$$

$$u\frac{\partial C}{\partial x} + v\frac{\partial C}{\partial y} = D\frac{\partial^2 C}{\partial y^2}. \tag{4}$$

The boundary conditions are given by

$$\begin{aligned} &u(x) = cx,\ v = -v_{\rm w},\ T = T_{\rm w}(x) = T_\infty + Ax^n,\\ &C = C_{\rm w},\ (y = 0),\\ &u \to U(x) = ax,\ T \to T_\infty,\\ &C \to C_\infty,\ (y \to \infty), \end{aligned} \tag{5}$$

where u and v are the velocity components along the x and y directions, respectively; T and C are, respectively, the temperature and concentration; $U(x)$ is the stagnation point velocity, K is the permeability of the porous medium, σ is the electric conductivity, B_0 is the magnetic induction, c_p is the specific heat at constant pressure, Q_0 is the volumetric heat generation/absorption rate, $q_{\rm r}$ is the radiative heat flux, D is the diffusion coefficient, ρ_∞ is the constant fluid density, n is the temperature parameter, and $v_{\rm w}$ represents suction velocity across the stretching sheet when $v_{\rm w} < 0$, and blowing when $v_{\rm w} > 0$. When $v_{\rm w} = 0$ the sheet is imbermeable. Following Prasad *et al.*,[30] the dynamic viscosity μ and the thermal conductivity k are given as

$$\frac{1}{\mu} = \frac{1}{\mu_\infty}[1 + \gamma(T - T_\infty)], \tag{6}$$

i.e.,

$$\begin{aligned} &\frac{1}{\mu} = a(T - T_{\rm r}),\\ &k = k_\infty[1 + \delta(T - T_\infty)], \end{aligned} \tag{7}$$

where $a = \gamma/\mu_\infty$, $T_{\rm r} = T_\infty - 1/\gamma$ are constants, and their values depend on the reference state and thermal property of the fluid; μ_∞ is the dynamic viscosity in the fluid free stream; k_∞ is the fluid free stream thermal conductivity, and δ is a constant depending on the nature of the fluid. By using the Rosseland diffusion approximation and following Hossain *et al.*,[14] the radiative heat flux $q_{\rm r}$ is given by

$$q_{\rm r} = \frac{-16\sigma^* T_\infty^3}{3k^*}\frac{\partial T}{\partial y}, \tag{8}$$

where σ^* is the Stefan–Boltzmann constant and k^* is the Rosseland mean absorption coefficient.

We now introduce the following relations for u, v, θ, and φ as

$$\begin{aligned} &u = \frac{\partial \psi}{\partial y},\ v = -\frac{\partial \psi}{\partial x},\ \theta = \frac{T - T_\infty}{T_{\rm w} - T_\infty},\\ &\varphi = \frac{C - C_\infty}{C_{\rm w} - C_\infty}, \end{aligned} \tag{9}$$

where ψ is the stream function, θ and φ are the non-dimensional temperature parameters. Using Eqs. (6)–(9) in the boundary layer Eqs. (2)–(4), we obtain the following equations:

$$\frac{\partial \psi}{\partial y}\frac{\partial^2 \psi}{\partial x \partial y} - \frac{\partial \psi}{\partial x}\frac{\partial^2 \psi}{\partial y^2} = U\frac{\partial U}{\partial U} + \frac{\theta_{\rm r}\nu_\infty}{\theta_{\rm r} - \theta}\frac{\partial^3 \psi}{\partial y^3} + \frac{\theta_{\rm r}}{(\theta - \theta_{\rm r})^2}\frac{\partial^2 \psi}{\partial y^2}\frac{\partial \theta}{\partial y} + \frac{\nu_\infty}{K}\frac{\theta_{\rm r}}{\theta_{\rm r} - \theta}\Big(U - \frac{\partial \psi}{\partial y}\Big) + \frac{\sigma B_0^2}{\rho_\infty}\frac{\partial \psi}{\partial y}, \tag{10}$$

$$\frac{\partial \psi}{\partial y}\Big(\frac{\partial \theta}{\partial x} + \frac{n\theta}{x}\Big) - \frac{\partial \psi}{\partial x}\frac{\partial \theta}{\partial y} = \frac{k_\infty}{\rho_\infty c_p}\Big[(1 + s\theta)\frac{\partial^2 \theta}{\partial y^2} + s\Big(\frac{\partial \theta}{\partial y}\Big)^2\Big] + \frac{16\sigma^* T_\infty^3}{3k^*\rho_\infty c_p}\frac{\partial^2 \theta}{\partial y^2} + \frac{Q_0}{\rho_\infty c_p}\theta, \tag{11}$$

$$\frac{\partial \psi}{\partial y}\frac{\partial \varphi}{\partial x} - \frac{\partial \psi}{\partial x}\frac{\partial \varphi}{\partial y} = D\frac{\partial^2 \varphi}{\partial y^2}, \tag{12}$$

where $s = \delta(T_{\rm w} - T_\infty)$ is the variable thermal conductivity parameter and $\theta_{\rm r} = -1/\gamma(T_{\rm w} - T_\infty)$ is the variable viscosity parameter.

The boundary conditions become

$$\begin{aligned} &\frac{\partial \psi}{\partial y} = cx,\ \frac{\partial \psi}{\partial y} = -v_{\rm w},\ \theta = 1,\ \varphi = 1,\ \ (y = 0),\\ &\frac{\partial \psi}{\partial y} = ax,\ \theta \to 0,\ \varphi \to 0,\ \ (y \to \infty). \end{aligned} \tag{13}$$

3. Solution of the problem

Firstly, we shall derive the similarity solutions using the Lie group method under which the non-linear differential equations (10)–(12) and boundary conditions (13) are invariant. The simplified form of the Lie-group transformation, namely the scaling group of transformations given by Layek *et al.*[31] are given by

$$\Gamma : x^* = x\,{\rm e}^{\varepsilon c_1},\ y^* = y\,{\rm e}^{\varepsilon c_2},\ \psi^* = \psi\,{\rm e}^{\varepsilon c_3},\ u^* = u\,{\rm e}^{\varepsilon c_4},\ v^* = v\,{\rm e}^{\varepsilon c_5},\ U^* = U\,{\rm e}^{\varepsilon c_6},\ \theta^* = \theta\,{\rm e}^{\varepsilon c_7},\ \varphi^* = \varphi\,{\rm e}^{\varepsilon c_8}, \tag{14}$$

where c_1, c_2, c_3, c_4, c_5, c_6, c_7, and c_8 are transformation parameters. Equation (14) is considered as a point-transformation transforming co-ordinates $(x, y, \psi, u, v, \theta, \varphi)$ into the coordinates $(x^*, y^*, \psi^*, u^*, v^*, \theta^*, \varphi^*)$. Substituting (14) into (10)–(12), we obtain

$$\begin{aligned} &\Big(\frac{\partial \psi^*}{\partial y^*}\frac{\partial^2 \psi^*}{\partial x^* \partial y^*} - \frac{\partial \psi^*}{\partial x^*}\frac{\partial^2 \psi^*}{\partial y^{*2}}\Big)\,{\rm e}^{\varepsilon(c_1 + 2c_2 - 2c_3)}\Big(1 - \frac{\theta^*\,{\rm e}^{-\varepsilon c_7}}{\theta_{\rm r}}\Big)^2\\ &\quad = \Big[U^*\frac{\partial U^*}{\partial x^*}\,{\rm e}^{\varepsilon(c_1 - 2c_6)} - \frac{\sigma B_0^2}{\rho_\infty}\frac{\partial \psi^*}{\partial y^*}\,{\rm e}^{\varepsilon(c_2 - c_3)}\Big]\Big(1 - \frac{\theta^*\,{\rm e}^{-\varepsilon c_7}}{\theta_{\rm r}}\Big)^2 + \Big[\nu_\infty\frac{\partial^3 \psi^*}{\partial y^{*3}}\,{\rm e}^{\varepsilon(3c_2 - c_3)}\end{aligned}$$

$$+\frac{\nu_\infty}{K}\Big(U^*\,\mathrm{e}^{-\varepsilon c_6}-\frac{\partial\psi^*}{\partial y^*}\,\mathrm{e}^{\varepsilon(c_2-c_3)}\Big)\Big]\Big(1-\frac{\theta^*\,\mathrm{e}^{-\varepsilon c_7}}{\theta_\mathrm{r}}\Big)+\frac{\nu_\infty}{\theta_\mathrm{r}}\frac{\partial\theta^*}{\partial y^*}\frac{\partial^2\psi^*}{\partial y^{*2}}\,\mathrm{e}^{\varepsilon(3c_2-c_3-c_7)}, \tag{15}$$

$$\Big[\frac{\partial\psi^*}{\partial y^*}\Big(\frac{\partial\theta^*}{\partial x^*}+\frac{n\theta^*}{x^*}\Big)-\frac{\partial\psi^*}{\partial x^*}\frac{\partial\theta^*}{\partial y^*}\Big]\,\mathrm{e}^{\varepsilon(c_1+c_2-c_3-c_7)}$$
$$=\frac{16\sigma^*T_\infty^3}{3k^*\rho_\infty c_p}\frac{\partial^2\theta^*}{\partial y^{*2}}\,\mathrm{e}^{\varepsilon(2c_2-c_7)}+\frac{Q_0}{\rho_\infty c_p}\theta^*\,\mathrm{e}^{-\varepsilon c_7}$$
$$+\frac{k_\infty}{\rho_\infty c_p}\Big[(1+s\theta^*\,\mathrm{e}^{-\varepsilon c_7})\frac{\partial^2\theta^*}{\partial y^{*2}}\,\mathrm{e}^{\varepsilon(2c_2-c_7)}+s\,\mathrm{e}^{2\varepsilon(c_2-c_7)}\Big(\frac{\partial\theta}{\partial y}\Big)^2\Big], \tag{16}$$

$$\Big(\frac{\partial\psi^*}{\partial y^*}\frac{\partial\phi^*}{\partial x^*}-\frac{\partial\psi^*}{\partial x^*}\frac{\partial\phi^*}{\partial y^*}\Big)\,\mathrm{e}^{\varepsilon(c_1+c_2-c_3-c_8)}=D\frac{\partial^2\phi^*}{\partial y^{*2}}\,\mathrm{e}^{\varepsilon(2c_2-c_8)}. \tag{17}$$

However, the system of Eqs. (15)–(17) remains invariant under the group of transformation Γ, if the following relations hold:

$$c_1+2c_2-2c_3=c_1+2c_2-2c_3-c_7=c_1+2c_2-2c_3-2c_7=c_1-2c_6=c_1-2c_6-c_7=c_1-2c_6-2c_7$$
$$=3c_2-c_3=3c_2-c_3-c_7=c_2-c_3=c_2-c_3-c_7=c_2-c_3-2c_7=-c_6=-c_6-c_7,$$
$$c_1+c_2-c_3-c_7=-c_7=2c_2-c_7=2c_2-2c_7,\ c_1+c_2-c_3-c_8=2c_2-c_8.$$

These relations give $c_1=c_3=c_4=c_6,\ c_2=c_5=c_7=c_8=0$. Thus, the set Γ reduces to a one-parameter group transformation as

$$\Gamma: x^*=x\,\mathrm{e}^{\varepsilon c_1},\ y^*=y,\ \psi^*=\psi\,\mathrm{e}^{\varepsilon c_1},\ u^*=u\,\mathrm{e}^{\varepsilon c_1}, v^*=v,\ U^*=U\,\mathrm{e}^{\varepsilon c_1},\ \theta^*=\theta,\ \varphi^*=\varphi. \tag{18}$$

Expanding by Taylor's method in powers of ε and keeping terms up to the order ε, we obtain

$$x^*-x=x\varepsilon c_1,\ y^*-y=0,\ \psi^*-\psi=\psi\varepsilon c_1,\ u^*-u=u\varepsilon c_1,\ v^*-v=0,\ U^*-U=U\varepsilon c_1,\ \theta^*-\theta=0,\ \varphi^*-\varphi=0.$$

After differentials, we yield

$$\frac{\mathrm{d}x}{c_1x}=\frac{\mathrm{d}y}{0}=\frac{\mathrm{d}\psi}{c_1\psi}=\frac{\mathrm{d}u}{c_1u}=\frac{\mathrm{d}v}{0}=\frac{\mathrm{d}U}{c_1U}=\frac{\mathrm{d}\theta}{0}=\frac{\mathrm{d}\varphi}{0}. \tag{19}$$

Solving the above equation, we obtain

$$\eta=y,\ \psi^*=xF(\eta),\ \theta^*=x\theta(\eta),\ \varphi^*=\varphi(\eta). \tag{20}$$

With the help of these relations, Eqs. (15)–(17) become

$$(F'^2-FF'')\Big(1-\frac{\theta}{\theta_\mathrm{r}}\Big)=a^2(1-\frac{\theta}{\theta_\mathrm{r}})^2+\nu_\infty\Big(1-\frac{\theta}{\theta_\mathrm{r}}\Big)F'''+\frac{\nu_\infty}{\theta_\mathrm{r}}F''\theta'-M^2\Big(1-\frac{\theta}{\theta_\mathrm{r}}\Big)^2F'$$
$$+\frac{\nu_\infty}{K}\Big(1-\frac{\theta}{\theta_\mathrm{r}}\Big)(a-F'), \tag{21}$$

$$nF'\theta-F\theta'=\frac{Q_0}{\rho_\infty c_p}\theta+\frac{16\sigma^*T_\infty^3}{3\rho_\infty c_pk^*}\theta''+\frac{k_\infty}{\rho_\infty c_p}\big[(1+s\theta)\theta''+s\theta'^2\big], \tag{22}$$

$$D\varphi''-F\varphi'=0. \tag{23}$$

The boundary conditions are transformed to

$$F'(\eta)=c,\ F(\eta)=-v_\mathrm{w},\ \theta(\eta)=1,\ \varphi(\eta)=1,\ \ (\eta=0);$$
$$F'(\eta)=a,\ \theta(\eta)\to0,\ \varphi(\eta)\to0,\ \ (\eta\to\infty). \tag{24}$$

Introducing the following transformations for η, F, θ, and φ in Eqs. (21)–(23), we have

$$\eta=\nu_\infty^\alpha c^b\eta^*,\quad F=\nu_\infty^{\alpha'}c^{b'}F^*,\quad \theta=\nu_\infty^{\alpha''}c^{b''}\theta^*,\quad \varphi=\nu_\infty^{\alpha'''}c^{b'''}\varphi^*.$$

Let $F^*=F$, $\theta^*=\theta$, and $\varphi^*=\varphi$. Eqs. (21)–(23) finally become

$$\Big(1-\frac{\theta}{\theta_\mathrm{r}}\Big)F'''-(F'^2-FF''-\lambda^2+M^2F')\Big(1-\frac{\theta}{\theta_\mathrm{r}}\Big)^2+\frac{\theta'}{\theta_\mathrm{r}}F''+k_1\Big(1-\frac{\theta}{\theta_\mathrm{r}}\Big)(\lambda-F')=0, \tag{25}$$

$$\Big(1+s\theta+\frac{4}{3}R\Big)\theta''+s\theta'^2+Pr\Big(1-\frac{\theta}{\theta_\mathrm{r}}\Big)(F\theta'+h\theta-nF'\theta)=0, \tag{26}$$

$$\varphi''+ScF\varphi'=0. \tag{27}$$

The corresponding boundary conditions take the form

$$F'(\eta)=1,\ F(\eta)=f_\mathrm{w},\ \theta(\eta)=1,\ \phi(\eta)=1,\ \ (\eta=0),$$
$$F'(\eta)=\lambda,\ \theta(\eta)\to0,\ \varphi(\eta)\to0,\ \ (\eta\to\infty), \tag{28}$$

where $\lambda = a/c$ is the velocity ratio parameter, $M = \sigma B_0^2/\rho_\infty c$ is the magnetic field, $k_1 = \nu_\infty/Kc$ is the permeability parameter of the porous medium, $Pr = (1-\theta/\theta_r)^{-1}Pr_\infty$ is the Prandtl number with $Pr_\infty = \mu_\infty c_p/k_\infty$ being the ambient Prandtl number, $R = 4\sigma T_\infty^3/k^* k_\infty$ is the thermal radiation parameter, $h = Q_0/\rho_\infty c_p$, c is the heat source parameter, $Sc = \nu_\infty/D$ is the Schmidt number and $f_w = -v_w/\sqrt{\nu_\infty c}$ is the dimensionless wall mass transfer coefficient such that $f_w > 0$ indicates wall suction and $f_w < 0$ indicates wall injection.

The set of non-linear ordinary differential Eqs. (25)–(27) with boundary conditions (28) have been solved by using the modified fourth-order Rung–Kutta method with systematic estimates of $F''(0)$, $\theta'(0)$ and $\varphi'(0)$ by the shooting technique.[32] In these calculations, the step size $\Delta\eta = 0.001$ while obtaining the numerical solution with $\eta_{max} = 10$ and five-decimal accuracy as the criterion for convergence. In the absence of diffusion equations, in order to validate our method, we compare the values of $F''(0)$ with the results obtained by Youssef *et al.*[29] for different values of λ and k_1 when we neglect the effects of θ_r, s, M, R, h, and f_w. As listed in Table 1, the two results are in excellent agreement with each other.

Table 1. Comparison of our result $F''(0)$ with that obtained from Ref. [29].

λ	$F''(0)$[29]				$F''(0)$ (our result)			
	$k_1=0$	$k_1=0.1$	$k_1=0.5$	$k_1=1$	$k_1=0$	$k_1=0.1$	$k_1=0.5$	$k_1=1$
0.1	−0.969643	−1.010073	−1.158373	−1.321118	−0.96938617	−1.01007010	−1.15833564	−1.32111138
0.2	−0.918164	−0.951899	−1.076833	−1.215624	−0.91810711	−0.95185914	−1.07682276	−1.21562277
0.5	−0.667259	−0.685439	−0.754013	−0.832126	−0.66726369	−0.68544264	−0.75401495	−0.83212614
2	2.017506	2.041796	2.136322	2.249105	2.01750275	2.04179517	2.13632005	2.24910390
3	4.729285	4.770855	4.933765	5.130383	4.72928226	4.77085184	4.93376134	5.13038093

The computations have been carried out for linear surface temperature variation for different values of velocity ratio parameter (λ), variable viscosity (θ_r), variable thermal conductivity (s), magnetic parameter (M), permeability parameter of the porous medium (k_1), thermal radiation (R), Schmidt number (Sc), and the dimensionless wall mass transfer (f_w). Numerical computations of the results are given in Figs. 1–20 to gain greater insight in the qualitative analysis of the results for $Pr = 0.71$, which represents air at temperature 20 °C and $Sc = 0.22$ corresponds to hydrogen that represents a diffusion chemical species of the most common items in air, as indicated by Gebhart *et al.*[33] Figures 1(a) and 1(b) show the respective changes in the viscosity function μ/μ_∞ and the thermal conductivity function k/k_∞ as the velocity ratio parameter λ is changed for two cases: (i) uniform viscosity ($\theta_r \to \infty$) and uniform thermal conductivity ($s = 0$), (ii) temperature viscosity ($\theta_r = 1.2$) and temperature dependent thermal conductivity ($s = 0.5$). In the case of variable fluid properties ($\theta_r = 1.2, s = 0.5$), an increase in the velocity ratio parameter λ obviously decreases the viscosity and thermal conductivity distributions and these approach unity at the outer edge of the boundary layer. In the absence of variable fluid properties ($\theta_r \to \infty, s = 0$), the velocity ratio parameter has a negligible effect on the viscosity and thermal conductivity distributions inside the boundary layer.

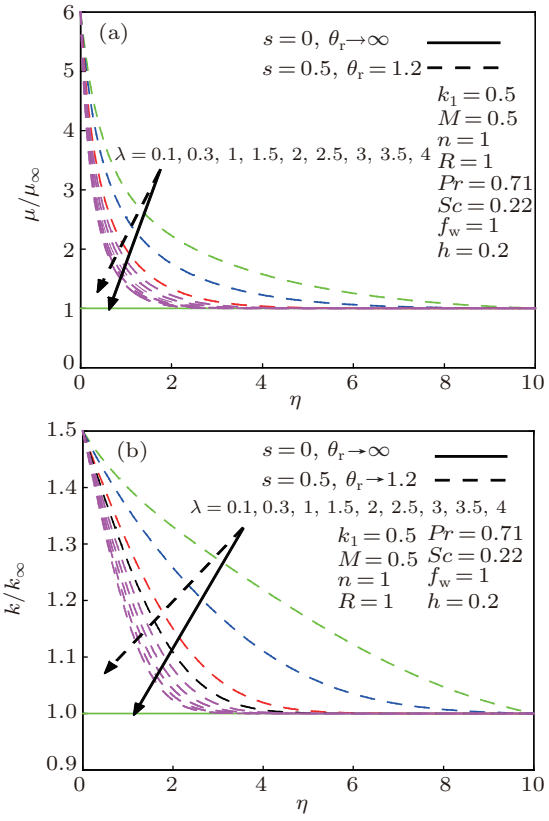


Fig. 1. (colour online) (a) Viscosity distribution for different values of λ. (b) Thermal conductivity distribution for different values of λ.

Figures 2–4 are the graphical representation of dimensionless velocity, temperature and concentration profiles for the same physical parameters used

in Fig. 1, for constant as well as for variable fluid properties. It is observed that the temperature and concentration decrease with increasing λ, but the velocity increases. In addition, the velocity in the case of constant fluid properties is higher than that of variable properties for all values of $\lambda > 1$. However, the opposite trend is seen for the temperature and concentration profiles. For $\lambda < 1$, the velocity in the case of constant fluid properties is lower than that of variable fluid properties and the reverse trend is seen for the temperature and concentration profiles. Note that no momentum or concentration boundary layer is formed when $\lambda = 1$, because the fluid velocity equals the velocity of the stretching sheet. It is worth mentioning that using the temperature-dependent viscosity and thermal conductivity for the case of fluid heating ($T_w > T_\infty$) gives a substantial error in the distribution of velocity, temperature and concentration. This error is shown in Figs. 2–4 by plotting the velocity, temperature and concentration profiles. Therefore, we conclude that for some kinds of mixtures (for example, H_2–air) of light or medium molecular weight, the variable viscosity and thermal conductivity effects should not be neglected.

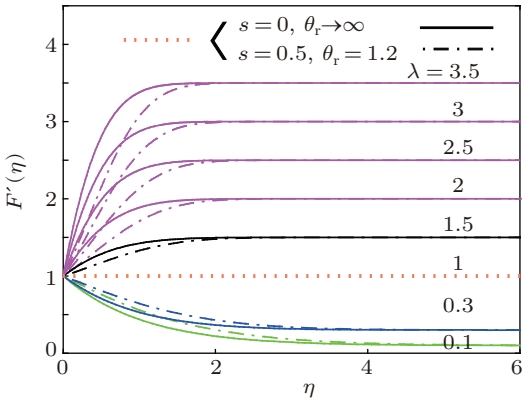


Fig. 2. (colour online) Velocity distribution for different values of λ, s, and θ_r.

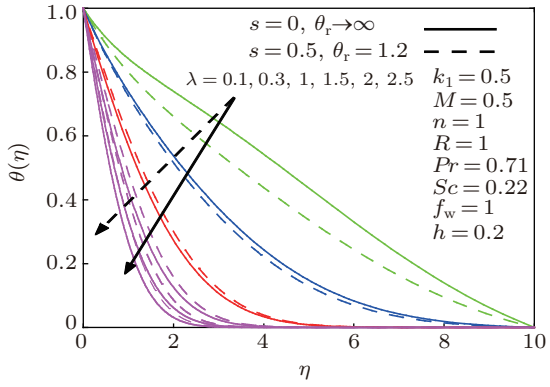


Fig. 3. (colour online) Temperature distribution for different values of λ, s, and θ_r.

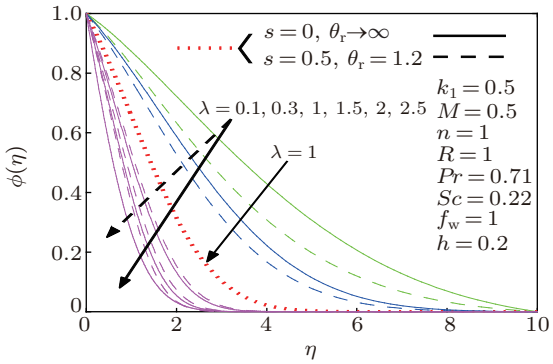


Fig. 4. (colour online) Concentration distribution for different values of λ, s, and θ_r.

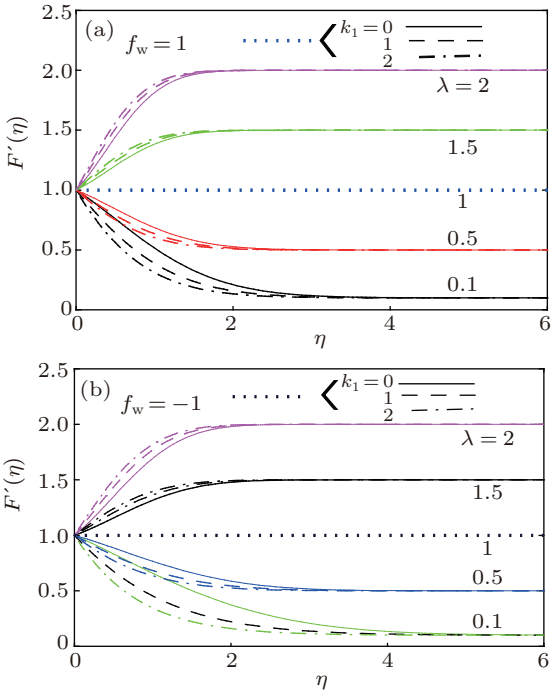


Fig. 5. (colour online) Velocity distribution for different values of λ and k_1. (b) Velocity distribution for different values of λ and k_1.

The effect of the porosity parameter k_1 on the velocity, temperature and concentration profiles for different values of the velocity ratio parameter λ are presented in Figs. 5–7 for both suction ($f_w > 0$) as well as injection ($f_w < 0$) cases with $\theta_r = 1.2$ and $s = 0.5$. We can see that for $\lambda < 1$, increasing in the value of k_1 will resist the flow. This, in turn, causes decreases in the velocity and increases in the temperature and concentration profiles. In addition, a reverse trend is seen in the case of $\lambda > 1$. The phenomenon for small ($\lambda < 1$) and large ($\lambda > 1$) values of λ has been explained by Layek *et al.*[31] Moreover, the influence of the porosity parameter k_1 is more pronounced for the case of injection ($f_w < 0$) than suction ($f_w > 0$) for both higher and lower values of the velocity ratio parameter λ. Furthermore, for $\lambda = 1$, the values of

the velocity, temperature and concentration are unaffected by the porosity parameter. This is because the free stream velocity is equal to the velocity of the stretching sheet.

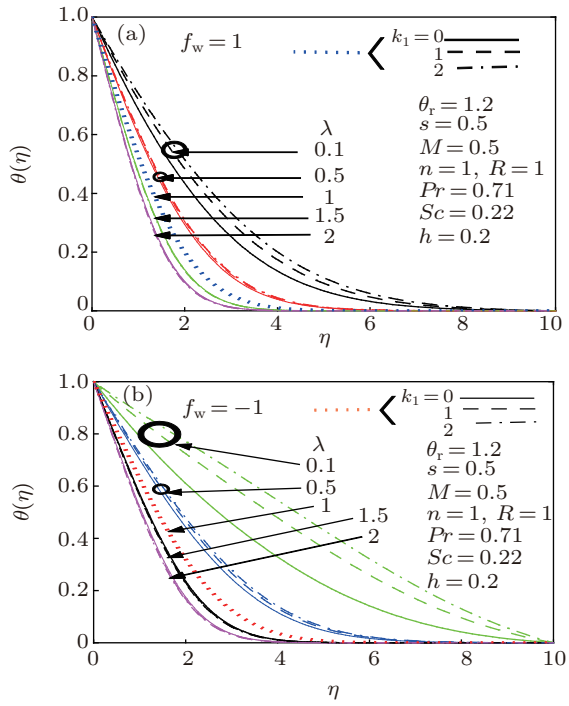


Fig. 6. (colour online) (a) Temperature distribution for different values of λ and k_1. (b) Temperature distribution for different values of λ and k_1.

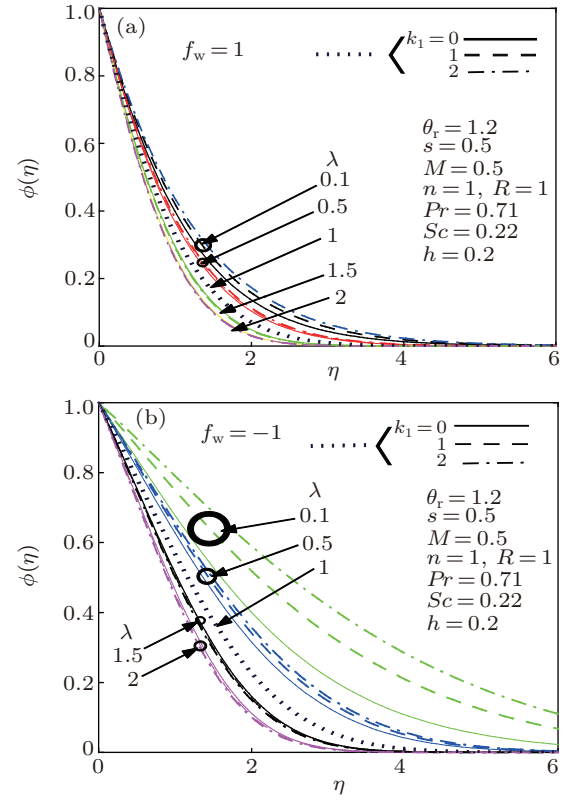


Fig. 7. (colour online) (a) Concentration distribution for different values of λ and k_1. (b) Concentration distribution for different values of λ and k_1.

Figures 8–10 show the effect of magnetic field parameter M in suction ($f_w > 0$) and injection ($f_w < 0$) cases on the dimensionless velocity, temperature, and concentration, for different values of λ with $\theta_r = 1.2$ and $s = 0.5$. The effect of M on the velocity, temperature, and concentration distributions depends on λ. For $\lambda > 1$ (the free stream velocity of the external stream exceeds the stretching velocity of the surface), the application of a magnetic field moving with the free stream has the tendency to induce a motive force which increases the motion of the fluid and decreases its boundary layer. This is accompanied by a slight decrease in the fluid temperature and concentration within the boundary layer. In addition, the imposition of the stretching velocity of the surface exceeds the free stream velocity and ($\lambda < 1$) produces the opposite effect, namely increases the fluid temperature and concentration and a decrease in its velocity distribution through out the boundary layer. Note that the maximum difference in the dimensionless velocity, temperature, and concentration distributions for various values of M occurs under smaller values of the velocity ratio parameter λ, and this difference is almost negligible for $\lambda = 1$. This is because the free stream velocity is equal to the velocity of the stretching sheet. Furthermore, the effect of the magnetic field parameter is more obvious for a fluid injection ($f_w < 0$) than for a fluid suction ($f_w > 0$); i.e., the imposition of wall fluid suction for this problem reduces the effect of the magnetic field.

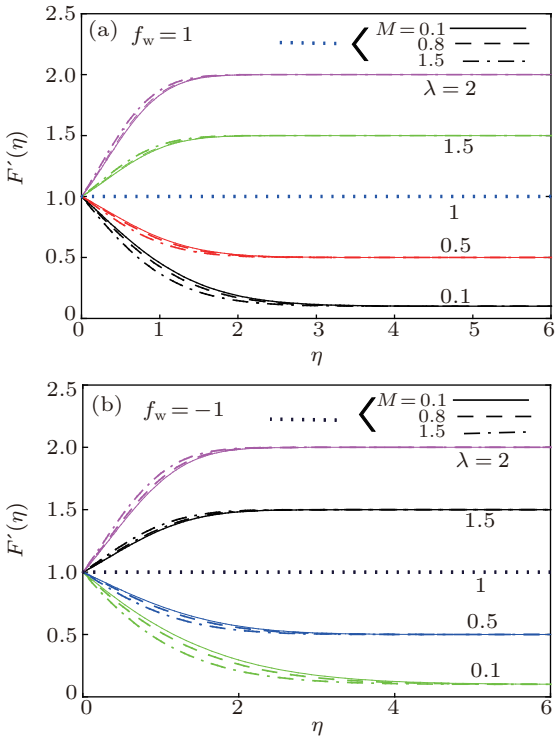


Fig. 8. (colour online) (a) Velocity distribution for different values of λ and M. (b) Velocity distribution for different values of λ and M.

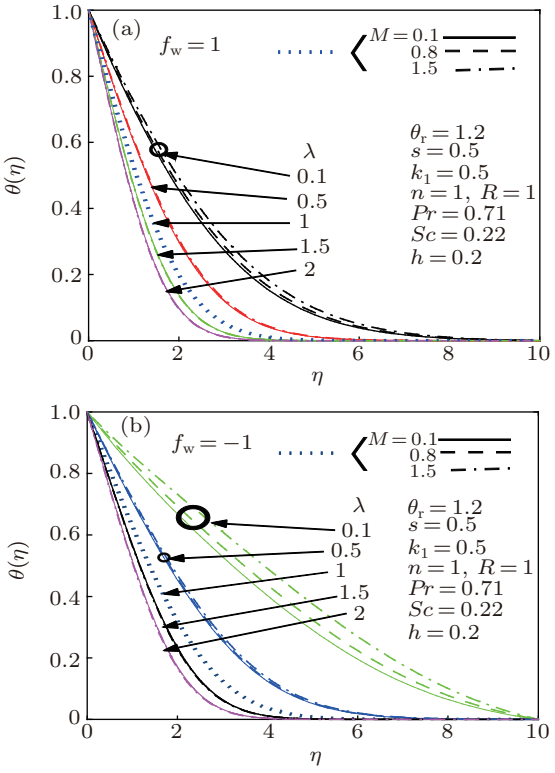


Fig. 9. (colour online) (a) Temperature distribution for different values of λ and M. (b) Temperature distribution for different values of λ and M.

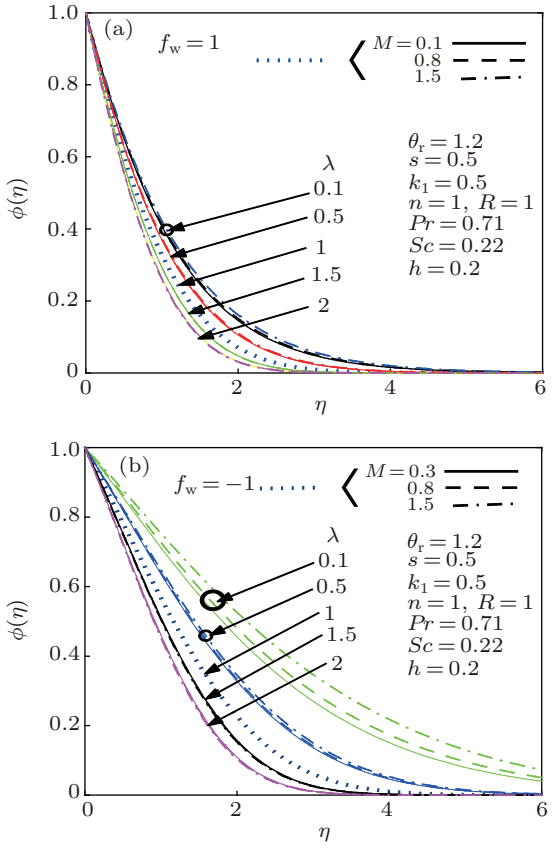


Fig. 10. (colour online) (a) Concentration distribution for different values of λ and M. (b) Concentration distribution for different values of λ and M.

Figures 11–13 show the effect of radiation parameter R on the velocity, temperature, and concentration profiles for three sets of values of λ (< 1, $= 1$, and > 1) with $\theta_r = 1.2$ and $s = 0.5$. For $\lambda < 1$, the velocity increases with the increasing the radiation parameter R, whereas the concentration profiles decrease as R increases. A reverse trend is also seen in the case of $\lambda > 1$. Furthermore, for $\lambda = 1$, the radiation parameter has no effect on the velocity and concentration distributions inside the boundary layer. It is very clear in Fig. 12 that the dimensionless temperature increases for all values of λ as R increases. This result qualitatively agrees with expectations since the effect of radiation is to increase the rate of energy transport to

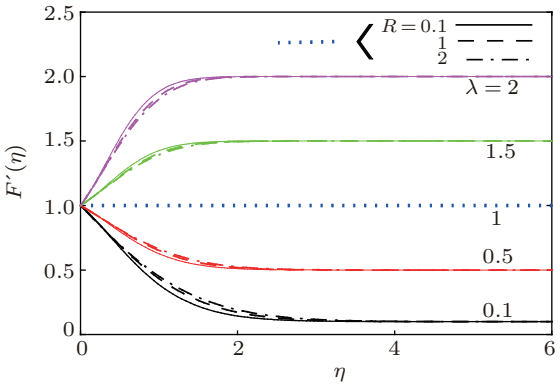


Fig. 11. (colour online) Velocity distribution for different values of λ and R.

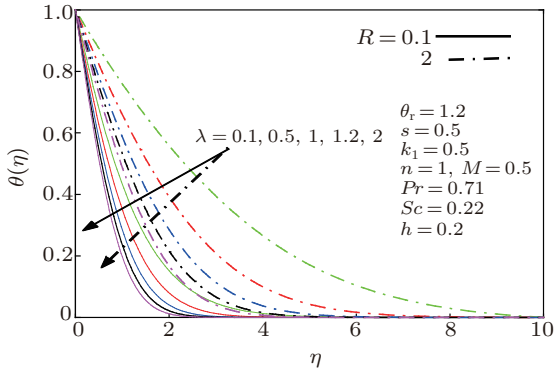


Fig. 12. (colour online) Temperature distribution for different values of λ and R.

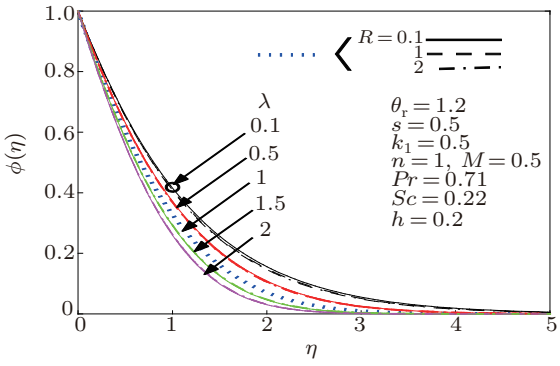


Fig. 13. (colour online) Concentration viscosity distribution for different values of λ and R.

the fluid, thus increasing the temperature of the fluid. In addition, the effect of radiation becomes more significant for a smaller velocity ratio parameter, as one can see from Fig. 12 by comparing the curves with $\lambda = 0.1$ and $\lambda = 2$.

Figure 14 shows the concentration profiles for different values of the velocity ratio parameter λ. The values of Schmidt number are chosen as 0.22, 0.78, and 0.94, which represent hydrogena Ammonia, and carbon dioxide, respectively, at 20 °C and 1 atmospheric pressure. It is observed that the concentration decreases with an increase in Schmidt number for both fluid suction and injection and for all the values of λ. This decrease in magnitude of concentration for carbon dioxide is lower than that of ammonia and hydrogen. Physically, this is possible because fluids with high species concentration have high viscosity and hence move slowly. The concentration profile is less affected by the velocity ratio parameter for $Sc = 0.94$. This behavior implies that the fluids having smaller Schmidt number are much more responsive to velocity ratio parameter than fluids having a larger Schmidt number. Furthermore, the effect of Sc is more pronounced for a fluid injection than for a fluid suction, i.e., the imposition of wall fluid suction for this problem reduces the effect of Schmidt number.

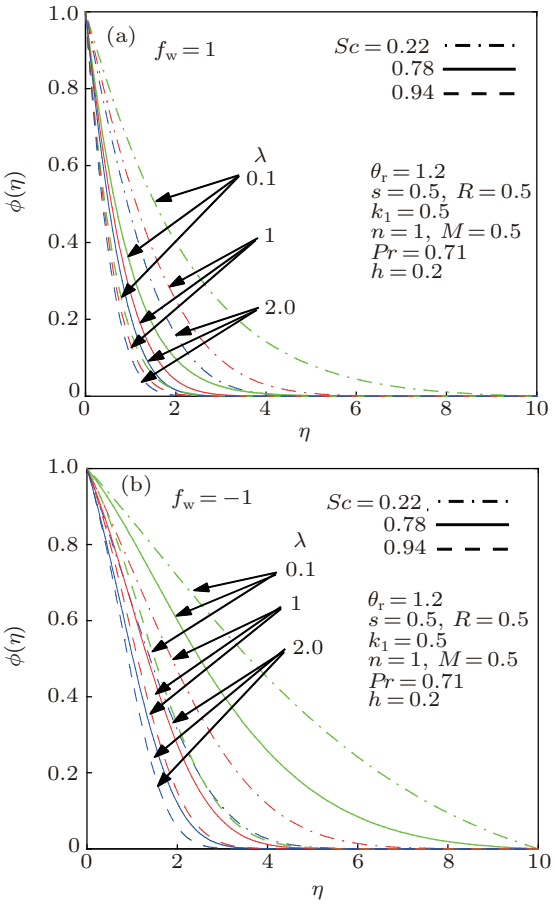


Fig. 14. (colour online) (a) Concentration distribution for different values of λ and Sc. (b) Concentration distribution for different values λ and Sc.

In Figs. 15–18, the effects of variable viscosity parameter θ_r on the wall shear stress $F''(0)$, the wall heat transfer $-\theta'(0)$ and the wall deposition flux $-\varphi'(0)$ are respectively presented for various values of the velocity ratio parameter λ for both suction ($f_w > 0$) and injection ($f_w < 0$) cases. The wall shear stress and the wall deposition flux decrease with increasing θ_r for both fluid suction and injection when $\lambda < 1$, while the reverse behavior is observed when $\lambda > 1$. For $\lambda = 1$, the values of $F''(0)$ are equal to zero and the values of $-\varphi'(0)$ remain constant for all values of θ_r. It is of interest to see the reversal of the sign of $F''(0)$ around $\lambda = 1$ for all values of θ_r. Physically, this point corresponds to zero friction in the boundary layer because the surface is stretching at the same velocity as the free stream. Before this point (i.e. for $\lambda < 1$), the stretching velocity of the surface exceeds the velocity of the external stream, so the boundary layer experiences negative friction. For $\lambda > 1$, the surface is stretching lower than the free stream, so the boundary layer experiences positive friction. From Fig. 16 we can see that the wall heat transfer increases as θ_r increases for fluid suction as well as for injection. We may also note that the wall heat transfer is greater for the suction case than for the injection case. Figures 18–20 show the wall shear stress $F''(0)$, the wall heat transfer $-\theta'(0)$ and the wall deposition flux $-\varphi'(0)$ against velocity ratio parameter λ for different values of magnetic field parameter M for both fluid suction and injection cases. These figures confirm that as M increases, the wall shear stress, the wall heat transfer and the wall deposition flux all decrease in the range $0 < \lambda < 1$, but increase in the range $1 < \lambda \leq 2$. This increase in $F''(0)$ is larger in the case of fluid suction. For $\lambda = 1$, the values of $F''(0)$ are equal to zero and the values of $-\theta'(0)$ and $-\varphi'(0)$ remain constant for all values of M when the sheet and the fluid move with the same velocity. These results are generally consistent with those in Figs. 8–10. Furthermore, we notice from these figures that for large values of the velocity ratio parameter $\lambda(\lambda > 1)$, the resistive effects of magnetic field are diminished; hence the wall shear stress increases with increasing M. The mass fluid suction ($f_w > 0$) is also found to enhance the effect of magnetic field parameter M in the boundary layer's flow field.

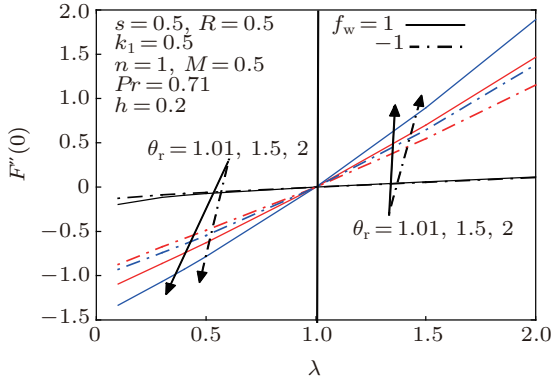


Fig. 15. (colour online) Wall shear stress for different values of λ, θ_r, and f_w.

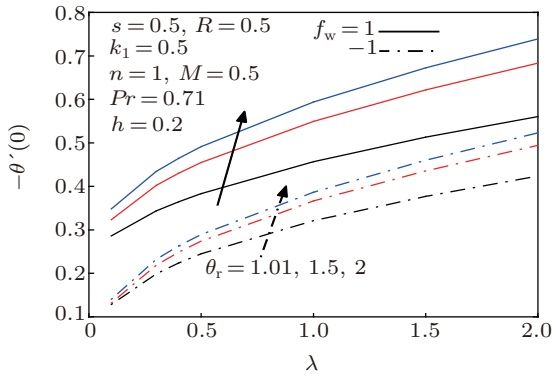


Fig. 16. (colour online) Wall heat transfer for different values of λ, θ_r, and f_w.

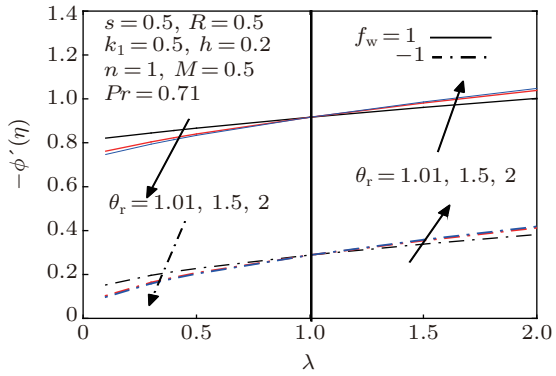


Fig. 17. (colour online) Wall deposition flux for different values of λ, θ_r, and f_w.

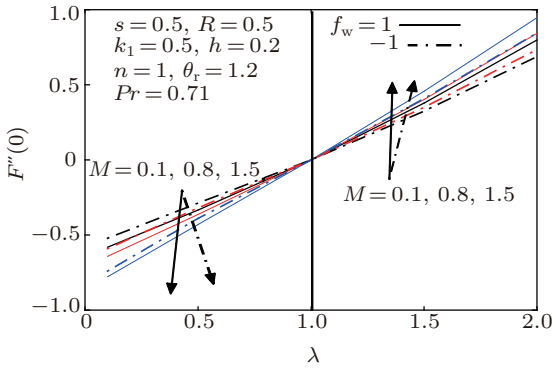


Fig. 18. (colour online) Wall shear stress for different values λ, M, and f_w.

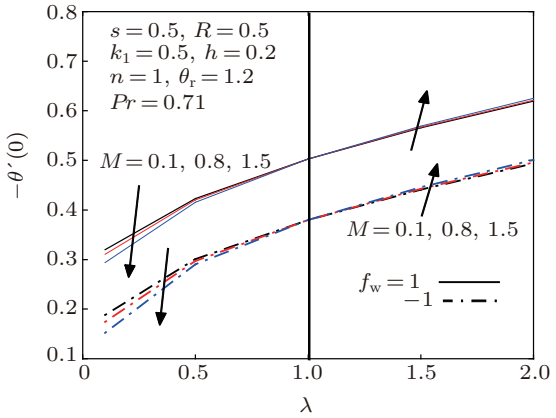


Fig. 19. (colour online) Wall heat transfer for different values of λ, M, and f_w.

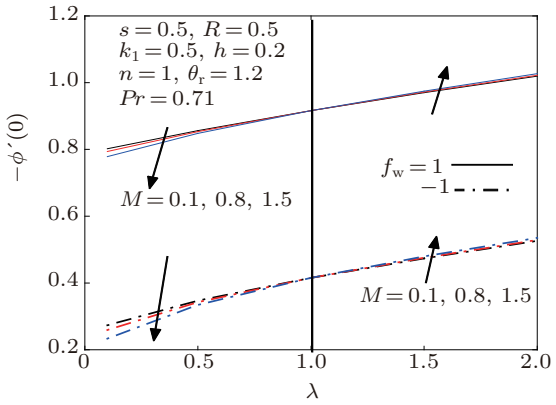


Fig. 20. (colour online) Wall deposition flux for different values of λ, M, and f_w.

4. Conclusion

In this work, the problem of combined heat and mass transfer in steady MHD two- dimensional stagnation-point flow in a porous medium of an incompressible viscous fluid towards a permeable stretching surface with variable viscosity and thermal conductivity in the presence of thermal radiation is investigated. The viscosity of the fluid is assumed to be an inverse linear function of temperature and the thermal conductivity is assumed to vary linearly with temperature. The stretching velocity and the surface temperature are assumed to vary linearly with the distance from the stagnation point. The governing equations for the problem were changed to dimensionless ordinary differential equations using a scaling group of transformations. The transformed governing equations in the present study were solved numerically by using the Rung–Kutta and shooting methods. The numerical results obtained agree very well with the previously published data for some particular cases of the present study. The results indicate that increasing the

velocity ratio parameter tends to increase the velocity profile but decrease the temperature and concentration profiles. In addition, when the variable viscosity and thermal conductivity are included, a considerable rise in the velocity profile and considerable reduction in the temperature and concentration profiles inside the boundary layer occur when $\lambda > 1$. However, the opposite behavior is found for $\lambda < 1$. When $\lambda = 1$, the velocity distribution near the stretching surface is the same as that away from the surface so that no boundary-layer is formed near the surface. Furthermore, the effect of magnetic field on the rate of shear stress may be reduced by suction but increased by injection when $\lambda < 1$, and the opposite is true when $\lambda > 1$. The rate of shear stress is found to be positive for $\lambda > 1$, negative for $\lambda < 1$, and zero for $\lambda = 1$. The imposition of fluid suction is to increase both the rate of heat and mass transfer, whereas injection shows the opposite effects.

References

[1] Hiemenz K 1911 *J. Dingl. Polytech.* **326** 321

[2] Eckart E R G 1942 *Die Berechnung des warmeuberg-angs in der laminaren Grenzschicht umstromter koper* VDI Forsch 416

[3] Ramachandran N, Chen T S and Armaly B F 1988 *ASME J. Heat Trans.* **110** 373

[4] Devi C D S, Tajhar H S and Nath G 1991 *Heat Mass Trans.* **26** 71

[5] Lok Y Y, Amin N, Campean D and Pop I 2005 *Int. J. Num. Methods Heat Fluid Flow* **15** 654

[6] Chiam T C 1994 *J. Phys. Soc. Jpn.* **63** 2443

[7] Mahapatra T R and Gupta A S 2001 *Acta Mech.* **152** 191

[8] Mahapatra T R and Gupta A S 2002 *Heat Mass Trans.* **38** 517

[9] Nazar R, Amin N, Filip D and Pop I 2004 *Int. J. Nonlinear Mech.* **39** 1227

[10] Nazar R, Amin N, Filip D and Pop I 2004 *Int. J. Eng. Sci.* **42** 1241

[11] Boutros Y Z, Abd-el Malek M B, Badran N A and Hassan H S 2006 *Meccanica* **41** 681

[12] Ishak A, Nazar R and Pop I 2006 *Magnetohydrodynamics* **42** 17

[13] Ishak A, Nazar R and Pop I 2006 *Meccanica* **41** 509

[14] Hossan M A and Takhar H S 1996 *Heat Mass Trans.* **31** 243

[15] Pop S R, Grosan T and Pop I 2004 *Technische Mechanick* **25** 100

[16] Layek G C, Mukhopadhyay S and Samad S K 2007 *Int. Comm. Heat Mass Trans.* **34** 347

[17] Dulal P 2009 *Meccanica* **44** 145

[18] Adrian P 2010 *Heat Mass Trans.* **46** 831

[19] Cebeci T and Bradshaw P 1984 *Physical and Computational Aspects of Convective Heat Transfer* (New York: Springer)

[20] Chamkha A J 2004 *Int. J. Eng. Sci.* **42** 217

[21] Seddeek M A and Salama F A 2007 *Comput. Mater. Sci.* **40** 186

[22] Salem A M 2007 *Phys. Lett.* A **369** 315

[23] Hassanian L A and Alarabi T H 2009 *Commun. Nonlinear Sci. Numer. Simulat.* **14** 1366

[24] Ibrahim F S, Mansour M A and Hamad M A A 2005 *Elect. J. Differential Eq.* **39** 1

[25] Ibrahim F S, Mansour M A and Hamad M A A 2007 *J. Egyption Math. Soc.* **15** 233

[26] Pandey M, Pandey M B D and Sharma V D 2009 *Appl. Math. Comp.* **215** 681

[27] Jalil M, Asghar S and Mushtaq M 2010 *Math. Prob. Eng.* **2010** 264901

[28] Hamad M A A and Ismail A I 2010 *Appl. Math. Sci.* (in press)

[29] Youssef Z B, Abdel-Malek M B, Badran N A and Hossam H S 2006 *Meccanica* **41** 681

[30] Prasad K V, Vajravelu K and Datti P S 2010 *Int. J. Thermal Sciences* **49** 603

[31] Layek G C, Mukhopadhyay S and Samad S K A 2006 *Math. Modeling and Analysis* **11** 187

[32] Na T Y 1979 *Computational Method in Engineering Boundary Value Problems* (New York: Academic press)

[33] Gebhart B, Jaluria Y, Mahajan R L and Summakia B 1988 *Buoyancy-Induced Flow and Transport* (New York: Hemisphere Pub. Group)